Design of a nonlinear absorber for a two degrees of freedom pendulum and experimental validation

Gabriel Hurel, Alireza Ture Savadkoohi, Claude-henri Lamarque

▶ **To cite this version:**

Gabriel Hurel, Alireza Ture Savadkoohi, Claude-henri Lamarque. Design of a nonlinear absorber for a two degrees of freedom pendulum and experimental validation. Structural Control and Health Monitoring, In press, 10.1002/stc.2814 . hal-03294253

HAL Id: hal-03294253
https://hal.science/hal-03294253

Submitted on 21 Jul 2021

HAL is a multi-disciplinary open access archive for the deposit and dissemination of scientific research documents, whether they are published or not. The documents may come from teaching and research institutions in France or abroad, or from public or private research centers.

L'archive ouverte pluridisciplinaire **HAL**, est destinée au dépôt et à la diffusion de documents scientifiques de niveau recherche, publiés ou non, émanant des établissements d'enseignement et de recherche français ou étrangers, des laboratoires publics ou privés.

Design of a nonlinear absorber for a two degrees of freedom pendulum and experimental validation

G. Hurel, A. Ture Savadkoohi, C.-H. Lamarque
Univ. Lyon, ENTPE, LTDS UMR 5513,
rue Maurice Audin, 69518 Vaulx-en-Velin
Email: gabriel.hurel@entpe.fr

Accepted on 24 June 2021

Abstract

A nonlinear energy sink is designed to control the oscillations of a two degrees-of-freedom pendulum under the following types of excitations: horizontal and vertical base displacements and initial energy. Coupled nonlinear governing system equations are treated with the multiple scale methods with different assumptions depending on applied loads. Fast and slow system dynamics are revealed leading to detection of different possible dynamical regimes. The choice of the design parameters of the nonlinear energy sink is discussed and a tuning method is proposed. The efficiency of the control is validated by an experimental study: a physical model of the pendulum is excited by the shake table. The response of the system shows that the nonlinear energy sink is able to control the main system.

Keywords passive control, nonlinear energy sink, pendulum, experimental validation

1 Introduction

In transportation systems, vibrations can be an issue for mechanical structures but also for passengers comfort. In order to control the vibrations of such systems, many types of devices are proposed. These control devices cover large categories of systems ranging between active, passive and hybrid ones [1]. In passive control systems, the most well-known device the tuned mass damper [2], which is a spring-mass system with the same natural frequency than the frequency of the targeted mode to be controlled. It has been shown that, via including a cubic non-linearity in the restoring forcing function of the spring, the efficiency of this device is improved [3]. In the nonlinear energy sink (NES) [4–6], the restoring force function is purely nonlinear, i.e. there is no linear component. This function can be polynomial, like the cubic function, or non-polynomial [7]. It is shown that the nonsmooth nonlinearity can be considered for the absorbers [7, 8]. Such systems are very efficient when the system possesses pre-stressing terms [9]. An example of such systems is the piece-wise linear one which can be built with a mass moving in a clearance between two linear springs or elastic barriers. The NES can be used in various domains such as civil engineering for buildings [10] or stay-cable [11, 12]. The passive control of a single degree-of-freedom (dof) pendulum by a tuned mass damper is studied by Matsuhisa et al. [13] The application of a NES with cubic and nonsmooth nonlinearities on controlling planar oscillations of a two dof pendulum under external excitations is studied by Hurel et al.[14, 15]. In addition, the same authors studied the control process of a single dof pendulum under base and external excitations

with cubic NES [16]. For the systems in gravitational field, the cubic NES looses its pure nonlinear nature due to the prestressing terms induced by the gravity. To overcome this fact, a nonsmooth NES can be used[17].

In this article, we propose a design procedure for controlling a two dof pendulum under two-dimensional base excitation (horizontal and vertical) and initial energies.

The paper is organized as it follows: In section 2, we present the system and its governing equations accompanied by some explanations about the principle of the NES. Then, in section 3, we tune the parameters to have a good and reasonable control. In section 4, an experimental validation is presented. At last, in section 5, the paper is concluded.

2 Principle of the nonlinear absorber

2.1 The main system: a two degrees-of-freedom pendulum

The mechanical system under consideration is a two dof pendulum of mass M in a gravity field $\vec{g} = -g\vec{k}$ shown in Figure 1. It is hung from a moving base O. The pendulum can rotates around $\vec{i}$ and $\vec{j}$ axes with angles ψ and φ respectively, transforming global reference frame $(\vec{i}, \vec{j}, \vec{k})$ in local reference frame $(\vec{i'}, \vec{j'}, \vec{k'})$. It is excited by the imposed displacement at its base O represented as $x_O(t)$, $y_O(t)$ and $z_O(t)$. The center of mass of the pendulum is located at the distance L from the base O. Viscous damping coefficients relative to the rotation of angles φ and ψ are represented as c_φ and c_ψ, respectively.

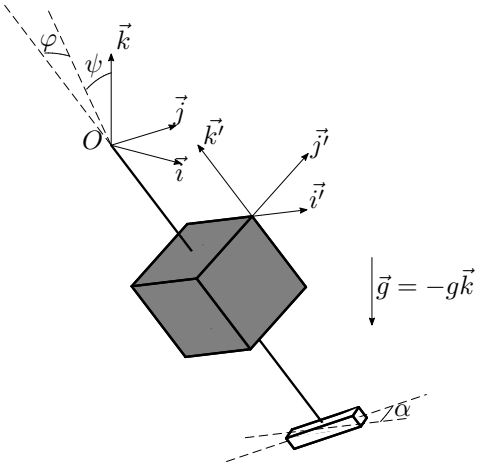

Figure 1: The main system: a two-degrees-of freedom pendulum under gravitational effects with $\vec{g} = -g\vec{k}$.

2.2 The nonlinear absorber

The control of the oscillations of the main system is made by a nonsmooth NES [8] coupled to the pendulum. The nonlinear absorber is composed of a mass m, moving in a guide between two linear springs of stiffness k, with a clearance of $2d$ (see Figure 2a). When its displacement $u = 0$, the mass is located at a distance a from the base O. The mass of the absorber is very small compared to the mass of the main system:

$$m = \varepsilon M, \varepsilon \ll 1 \tag{1}$$

In order to control the system in both directions, the NES is set to have an angle α with the axis $\vec{i'}$ as seen on Figure 2a. The restoring force function s of the NES is depicted in Figure 2b as a function of the displacement u of the mass m relative to the pendulum.

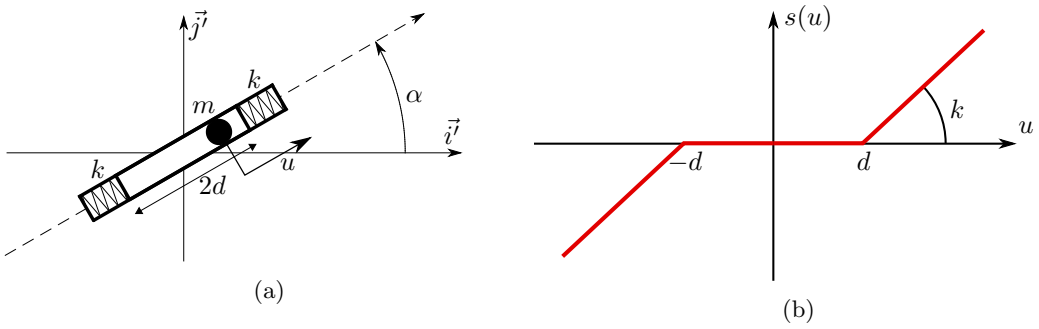

Figure 2: Nonsmooth NES: a) schematic of the piece-wise linear absorber; b) The restoring forcing function of the absorber.

2.3 Equations of the system

The kinetic ($\mathcal{K}$) and potential ($\mathcal{U}$) energies of the system read [15]:

$$\mathcal{K} = \frac{1}{2}M\left(\dot{x}_G^2 + \dot{y}_G^2 + \dot{z}_G^2\right) + \frac{1}{2}I_{xx}\dot{\varphi}^2 + \frac{1}{2}I_{yy}\dot{\psi}^2 + \frac{1}{2}m\left(\dot{x}_m^2 + \dot{y}_m^2 + \dot{z}_m^2\right) \tag{2}$$

$$\mathcal{U} = g(Mz_G + mz_m) + \mathcal{S}(u) \tag{3}$$

where $\dot{\bullet}$ stands for the time derivation of the variable $\bullet$, (x_G, y_G, z_G) are the coordinates of the center of mass G of the main system and (x_m, y_m, z_m) are the coordinates of the NES in the main reference of frame, I_{yy} and I_{xx} are the product of inertia of the main system around $\vec{i}$ and $\vec{j}$, respectively, and $\nabla\mathcal{S}(u) = s(u)$, where ∇ stands for the gradient operator. The non-conservatives forces applied on the system are:

$$F_\varphi = -c_\varphi\dot{\varphi} \tag{4}$$

$$F_\psi = -c_\psi\dot{\psi} \tag{5}$$

$$F_u = -c_u\dot{u} \tag{6}$$

The equations of the system are obtained with the Euler-Lagrange equations. They are provided in appendix A.

2.4 Assumptions

The main system is a two-dof system with generalized coordinates represented as φ and ψ. If we linearize the system around its equilibrium state ($\varphi = \psi = 0$), we can calculate two eigenmodes with the natural frequencies represented as ω_φ and ω_ψ. Because of the geometry and the inertia of the pendulum, we assume that the natural frequencies are close to each other:

$$\omega_\varphi = \omega_\psi + \sigma_\omega\varepsilon \tag{7}$$

We assume also that the displacement of the base O is periodic and its fundamental frequency is close to the natural frequencies of the main system:

$$x_O(t) = \sum_{j=0}^{\infty} x_j \mathrm{e}^{ij\Omega t} \tag{8}$$

$$y_O(t) = \sum_{j=0}^{\infty} y_j \mathrm{e}^{ij\Omega t} \tag{9}$$

$$z_O(t) = \sum_{j=0}^{\infty} z_j \mathrm{e}^{ij\Omega t} \tag{10}$$

where $i^2 = -1$ and $\Omega = \omega_\varphi + \sigma_\varphi \varepsilon = \omega_\psi + \sigma_\psi \varepsilon$. Finally, we assume that the angles and the displacements are small: $\varphi = \sqrt{\varepsilon}\underline{\varphi}$, $\psi = \sqrt{\varepsilon}\underline{\psi}$, $u = \sqrt{\varepsilon}\underline{u}$, $x_j = \varepsilon\sqrt{\varepsilon}\underline{x}_j$, $y_j = \varepsilon\sqrt{\varepsilon}\underline{y}_j$ and $z_j = \sqrt{\varepsilon}\underline{z}_j$. This type of scaling of system variables with respect to the ε parameter is not unique and it can vary depending on the nature of the problem (e.g. the type of excitation) [14–16].

Table 1 collects numerical values of system parameters which will be used in all numerical examples of this paper.

Table 1: Parameters of the considered system for all presented examples.

Part	**Parameter**	**Value**
Pendulum	g	$9.81\,\mathrm{m\,s^{-2}}$
	M	$1.68\,\mathrm{kg}$
	L	$0.10\,\mathrm{m}$
	ω_φ	$8.29\,\mathrm{rad\,s^{-1}}$
	ω_ψ	$8.42\,\mathrm{rad\,s^{-1}}$
	c_φ	$0.05\,\mathrm{N\,m\,rad^{-1}\,s^{-1}}$
	c_ψ	$0.05\,\mathrm{N\,m\,rad^{-1}\,s^{-1}}$
NES	m	$0.08\,\mathrm{kg}$
	a	$0.207\,\mathrm{m}$
	α	$\frac{\pi}{4}$
	k	$120\,\mathrm{N\,m^{-1}}$
	d	$0.02\,\mathrm{m}$
	c_u	$2.5\,\mathrm{N\,m^{-1}\,s^{-1}}$

2.5 Detection of fast/slow dynamics: complexification and multiple scale method

We introduce the complex variables of Manevitch [18]:

$$\Phi \mathrm{e}^{i\Omega t} = \dot{\underline{\varphi}} + i\Omega\underline{\varphi} \tag{11}$$

$$\Psi \mathrm{e}^{i\Omega t} = \dot{\underline{\psi}} + i\Omega\underline{\psi} \tag{12}$$

$$\mathrm{U} \mathrm{e}^{i\Omega t} = \dot{\underline{u}} + i\Omega\underline{u} \tag{13}$$

In the multiple time scale method [19], we consider that the time can be decomposed into fast (τ_0) and slow ($\tau_j, j = 1, 2, ...$) time scales.

$$\tau_0 = \varepsilon^0 t,\ \tau_1 = \varepsilon^1 t,\ \tau_2 = \varepsilon^2 t... \tag{14}$$

Then, the derivation operator is redefined as:

$$\frac{\mathrm{d}}{\mathrm{d}t} = \frac{\partial}{\partial \tau_0} + \varepsilon^1 \frac{\partial}{\partial \tau_1} + \varepsilon^2 \frac{\partial}{\partial \tau_2} + ... \tag{15}$$

In this analysis, we keep only the first harmonics of the response of the system. This is done for an arbitrary function of the system $h(\tau_0, \tau_1, \tau_2...)$ by following operator:

$$H = \frac{\Omega}{2\pi} \int_0^{\frac{2\pi}{\Omega}} h(\tau_0, \tau_1, \tau_2...) \mathrm{e}^{-i\Omega\tau_0} \mathrm{d}\tau_0 \tag{16}$$

Applying Equation 16, we assume that Φ, Ψ and U are independent of fast time scale τ_0. This will be verified during multiple scale method or we will look at an asymptotic system

behavior where fast time (τ_0) tends to infinity. After applying equations 11-13 and 16 on governing system equations, following system is obtained:

$$Lg\frac{\mathrm{d}\Phi}{\mathrm{d}\tau_0}+i\frac{Lg(\Omega^2-\omega_\varphi^2)}{2\Omega}\Phi+\varepsilon\omega_\varphi^2\left[a^2\frac{\mathrm{d}\Phi}{\mathrm{d}\tau_0}+\frac{Lg}{\omega_\varphi^2}\frac{\mathrm{d}\Phi}{\mathrm{d}\tau_1}+a\cos(\alpha)\frac{\mathrm{d}U}{\mathrm{d}\tau_0}+\left(\frac{\underline{c}_\varphi+ia^2\Omega}{2}-i\frac{ag}{2\Omega}\right)\Phi\right.$$
$$+i\frac{Lg}{16\Omega^3}|\Phi|\,\Phi+i\frac{a\Omega^2-g}{2\Omega}\cos(\alpha)U+iL\left(\frac{L}{8\Omega}+\frac{g}{16\Omega^3}\right)\Psi^2\Phi^*-i\frac{L^2}{4\Omega}\Phi\,|\Psi|+i\frac{Lg}{8\Omega^3}\Phi\,|\Psi|$$
$$\left.-L\Omega^2x_1-2iL\Omega z_2\Phi^*\right]+O(\varepsilon^2)=0 \tag{17}$$

$$Lg\frac{\mathrm{d}\Psi}{\mathrm{d}\tau_0}+i\frac{Lg(\Omega^2-\omega_\psi^2)}{2\Omega}\Psi+\varepsilon\omega_\psi^2\left[a^2\frac{\mathrm{d}\Psi}{\mathrm{d}\tau_0}+\frac{Lg}{\omega_\psi^2}\frac{\mathrm{d}\Psi}{\mathrm{d}\tau_1}+a\sin(\alpha)\frac{\mathrm{d}U}{\mathrm{d}\tau_0}+\left(\frac{\underline{c}_\psi+ia^2\Omega}{2}-i\frac{ag}{2\Omega}\right)\Psi\right.$$
$$+i\frac{Lg}{16\Omega^3}|\Psi|\,\Psi+i\frac{a\Omega^2-g}{2\Omega}\sin(\alpha)U+iL\left(\frac{L}{8\Omega}+\frac{g}{16\Omega^3}\right)\Phi^2\Psi^*-i\frac{L^2}{4\Omega}\Psi\,|\Phi|+i\frac{Lg}{8\Omega^3}\Psi\,|\Phi|$$
$$\left.-L\Omega^2y_1-2iL\Omega z_2\Psi^*\right]+O(\varepsilon^2)=0 \tag{18}$$

$$\varepsilon\left[\frac{\mathrm{d}U}{\mathrm{d}\tau_0}+a\cos(\alpha)\left(\frac{\mathrm{d}\Phi}{\mathrm{d}\tau_0}-\frac{gi}{2a\Omega}\Phi+\frac{\Omega i}{2}\Phi\right)+a\sin(\alpha)\left(\frac{\mathrm{d}\Psi}{\mathrm{d}\tau_0}-\frac{gi}{2a\Omega}\Psi+\frac{\Omega i}{2}\Psi\right)+\frac{\lambda+\Omega i}{2}U-i\frac{K}{2\Omega}\mathrm{U}S(|\mathrm{U}|)\right]+O(\varepsilon^2) \tag{19}$$

with $\underline{c}_\varphi=\dfrac{c_\varphi}{m}$, $\underline{c}_\psi=\dfrac{c_\psi}{m}$ and

$$S(|\mathrm{U}|)=\frac{2}{\pi}\begin{cases}0 & \text{if } |\mathrm{U}|\le D\\ \arccos\left(\dfrac{D}{|\mathrm{U}|}\right)-\dfrac{D\sqrt{|\mathrm{U}|^2-D^2}}{|\mathrm{U}|^2} & \text{if } |\mathrm{U}|>D\end{cases} \tag{20}$$

where $\lambda=\dfrac{c_u}{m}$, $D=\dfrac{\Omega d}{\sqrt{\varepsilon}}$ and $K=\dfrac{k}{m}$ [7].

2.6 Analysis of the system

At the first order $O(\varepsilon^0)$, corresponding to the fast time scale τ_0, the equations of the system read:

$$\frac{\partial\Phi}{\partial\tau_0}=0 \tag{21}$$

$$\frac{\partial\Psi}{\partial\tau_0}=0 \tag{22}$$

$$\frac{\partial\mathrm{U}}{\partial\tau_0}+a\cos(\alpha)\frac{\partial\Phi}{\partial\tau_0}+a\sin(\alpha)\frac{\partial\Psi}{\partial\tau_0}+i\frac{A}{2\Omega}\left(\cos(\alpha)\Phi+\sin(\alpha)\Psi\right)+\frac{i\Omega+\lambda}{2}\mathrm{U}-i\frac{K}{2\Omega}\mathrm{U}S(|\mathrm{U}|)=0 \tag{23}$$

with $A=(a\Omega^2-g)$. We express the complex variables in polar form: $\Phi=N_\varphi\mathrm{e}^{i\delta_\varphi}$, $\Psi=N_\psi\mathrm{e}^{i\delta_\psi}$ and $\mathrm{U}=N_u\mathrm{e}^{i\delta_u}$. We seek for an asymptotic state when τ_0 tends to infinity, i.e., $\dfrac{\partial\mathrm{U}}{\partial\tau_0}\longrightarrow 0$. Equation 23 gives the expression of the slow invariant manifold (SIM):

$$\cos^2(\alpha)N_\varphi^2+\sin^2(\alpha)N_\psi^2+2\sin(\alpha)\cos(\alpha)\cos(\delta)N_\varphi N_\psi=\frac{\left(KS(N_u)-\Omega^2\right)^2+\lambda^2\Omega^2}{A^2}N_u^2 \tag{24}$$

where $\delta=\delta_\varphi-\delta_\psi$. The SIM is function of four real variables N_φ, N_ψ, N_u and δ. It can be represented in the space (N_φ,N_ψ,N_u) for several values of δ. The SIM is composed of

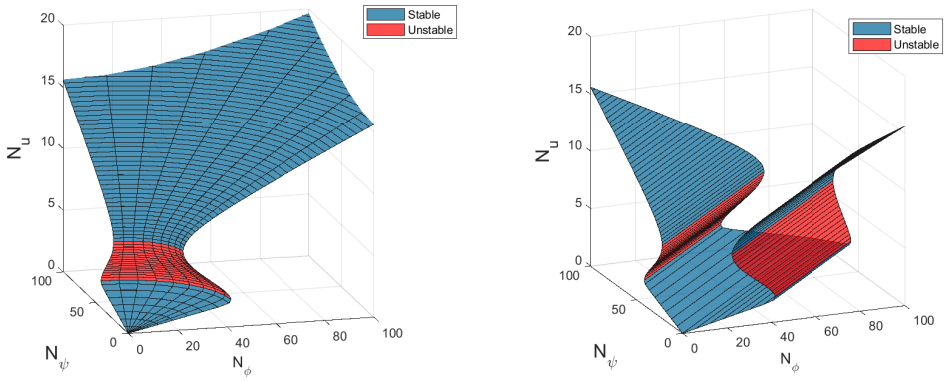

(a) $\delta = 0.5\pi$ (b) $\delta = \pi$

Figure 3: The three-dimensional views of the SIM for two values of δ.

stable and unstable zones delimited by singular points as demonstrated in [15]. Figure 3 shows the SIM with stable and unstable zones for an arbitrary value of δ and a particular value $\delta = \pi$.

The ε^1 order of equations corresponding to the slow time scale τ_1, yields to:

$$\begin{aligned} Lg\frac{\partial \Phi}{\partial \tau_1} =& \underline{x}_1 L\Omega^4 + 2i\underline{z}_2 L\Omega^3 \Phi^* - \left(i\frac{2\sigma_\varphi Lg}{2} + \frac{\underline{c}_\varphi \Omega^2}{2}\right)\Phi - i\frac{A\Omega}{2}\left(a\Phi + \cos(\alpha)\mathrm{U}\right) \\ & - i\frac{Lg}{16\Omega}\left[|\Phi|^2\Phi + \left(2 - \frac{4L\Omega^2}{g}\right)\Phi|\Psi|^2 + \left(Lg + \frac{2L\Omega^2}{g}\right)\Phi^*\Psi^2\right] \end{aligned} \tag{25}$$

$$\begin{aligned} Lg\frac{\partial \Psi}{\partial \tau_1} =& \underline{y}_1 L\Omega^4 + 2i\underline{z}_2 L\Omega^3 \Psi^* - \left(i\frac{2\sigma_\psi Lg}{2} + \frac{\underline{c}_\psi \Omega^2}{2}\right)\Psi - i\frac{A\Omega}{2}\left(a\Psi + \sin(\alpha)\mathrm{U}\right) \\ & - i\frac{Lg}{16\Omega}\left[|\Psi|^2\Psi + \left(2 - \frac{4L\Omega^2}{g}\right)\Psi|\Phi|^2 + \left(Lg + \frac{2L\Omega^2}{g}\right)\Psi^*\Phi^2\right] \end{aligned} \tag{26}$$

2.7 Different cases of excitations

We identify three cases of excitations for which the NES can control the pendulum oscillations:

- Horizontal base excitation
- Initial energy
- Vertical base excitation

These different excitation types are considered separately in following sections in order to simplify and also to solve Equations 25 and 26.

2.7.1 Horizontal base excitation

In this case, there is a horizontal periodic motion of the base O. The NES is designed to keep the amplitude of the main system below a given threshold. For design, it is necessary to know either the maximal amplitude of excitation to find the lowest threshold, or the maximal amplitude of the main system allowed to be effective at the highest excitation amplitude. In this study, we suppose that we know the maximum amplitude of excitation.

We assume that excitation and complex variables are small. A second rescaling is performed: $\underline{x}_1 = \sqrt{\varepsilon}X_1$, $\underline{y}_1 = \sqrt{\varepsilon}Y_1$, $\underline{z}_2 = \sqrt{\varepsilon}Z_2$, $\Phi = \sqrt{\varepsilon}\underline{\Phi}$, $\Psi = \sqrt{\varepsilon}\underline{\Psi}$, $\mathrm{U} = \sqrt{\varepsilon}\underline{\mathrm{U}}$ and $D = \sqrt{\varepsilon}\underline{D}$.

The effect of the vertical displacement of the base O is no more visible at this order. The equilibrium points are obtained via setting $\dfrac{\partial \Phi}{\partial \tau_1} = 0$ and $\dfrac{\partial \Psi}{\partial \tau_1} = 0$ in Equation 25 and 26 accompanied by consideration of the Equation of the SIM (24):

$$X_1 L\Omega^4 - \left(i\frac{2\sigma_\varphi Lg}{2} + \frac{\underline{c}_\varphi \Omega^2}{2} \right) \underline{\Phi} - i\frac{A\Omega}{2} \left(a\underline{\Phi} + \cos(\alpha)\underline{\mathrm{U}} \right) = 0 \tag{27}$$

$$Y_1 L\Omega^4 - \left(i\frac{2\sigma_\psi Lg}{2} + \frac{\underline{c}_\psi \Omega^2}{2} \right) \underline{\Psi} - i\frac{A\Omega}{2} \left(a\underline{\Psi} + \sin(\alpha)\underline{\mathrm{U}} \right) = 0 \tag{28}$$

In order to determinate the efficiency of the NES for a given excitation, we calculate the equilibrium points of the system for a range of frequency in the interval $\Omega \in [\omega_{\min}, \omega_{\max}]$. Figure 4 shows that N_φ, N_ψ and N_u of the equilibrium points of the system with NES are lower than the system without NES. We can also see that for some values of the frequency Ω there is no stable equilibrium point. These zones can correspond to different non periodic responses such as strongly modulated response (SMR) [14, 20] which is due to existence of fold singularities in the system. Figure 5 shows that the system oscillates between both stable zone of the SIM. The amplitudes N_φ and N_ψ oscillate and stay below a threshold.

However, as the SIM has dimension four, which creates difficulty in its visualization. That's why analytical predictions should be compared carefully with results obtained from direct numerical integration of the system equations.

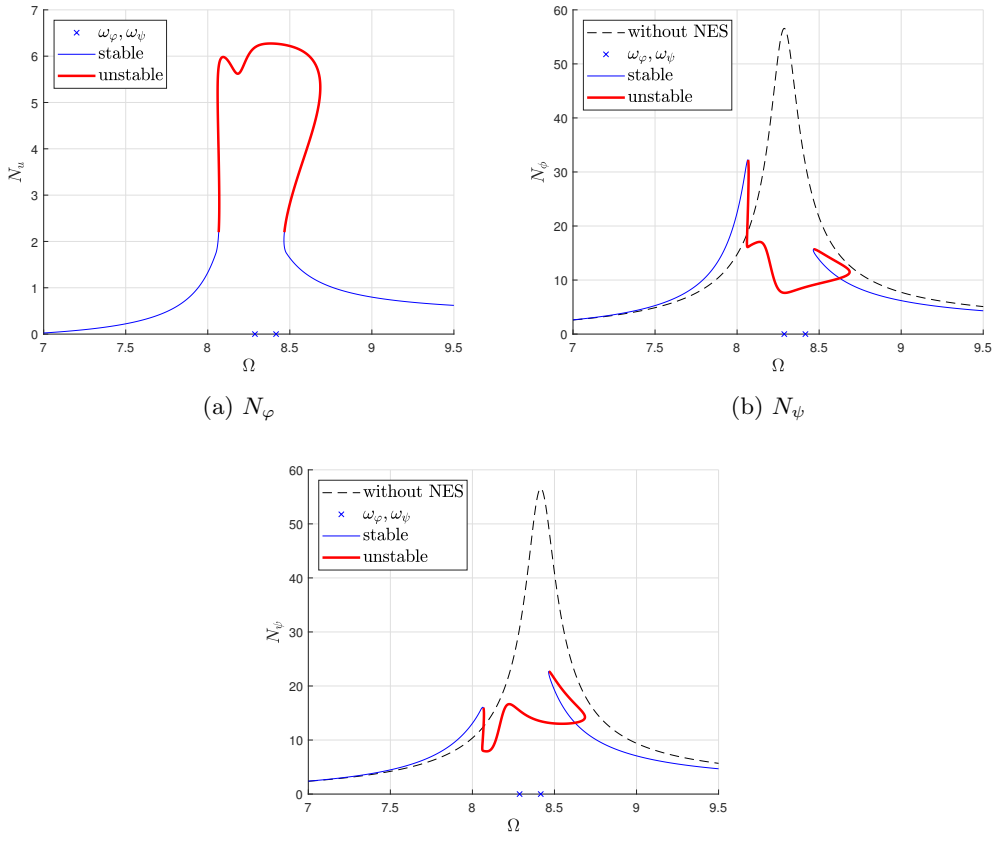

(a) N_φ (b) N_ψ

(c) N_u

Figure 4: Equilibrium points of the system for a horizontal excitation $x_1 = 17\,\mathrm{mm}$.

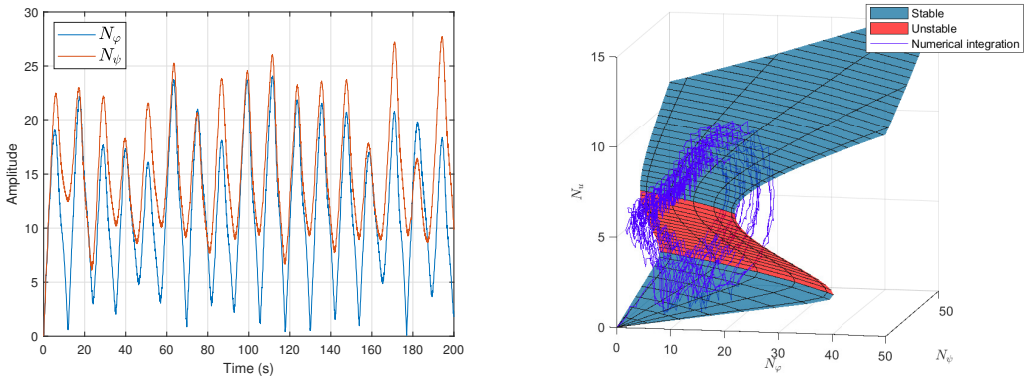

(a) Amplitude of the system

(b) Numerical results with the SIM

Figure 5: Numerical results showing SMR type oscillations of the system $x_1 = 13.5\,\text{mm}$ and $\Omega = 8.5$.

2.7.2 The system under initial energy

In this case, the base O is motionless but an initial energy is applied to the mass M of the pendulum. This energy can be due to a sudden displacement of O. The role of the NES is to absorb this energy rapidly. Here, the time t_c to reach a given amplitude from an initial amplitude of pendulum is a criterion to be minimized for tuning the NES.

Without excitation, we can observe from Equations 25 and 26 that the only equilibrium point of the system is $\Phi = \Psi = 0$. We have to evaluate the decreasing speed of the amplitude. We introduce the new complex variable: $\Theta = \cos(\alpha)\underline{\Phi} + \sin(\alpha)\underline{\Psi}$. By considering almost equal damping scenarios for the system as: $\underline{c}_\theta = \underline{c}_\varphi + \varepsilon\sigma_{c_\varphi} = \underline{c}_\psi + \varepsilon\sigma_{c_\psi}$ and very close frequency $\sigma_\theta = \sigma_\varphi + \varepsilon\sigma_{\sigma_\varphi} = \sigma_\psi + \varepsilon\sigma_{\sigma_\psi}$, the Equations 27 and 28 give:

$$\frac{\partial\Theta}{\partial\tau_1} = -\left(i\sigma_\theta + \frac{\underline{c}_\theta\Omega^2 + i\Omega aA}{2Lg}\right)\Theta - i\frac{\Omega A}{2Lg}\mathrm{U} \tag{29}$$

Equation 23 becomes:

$$A\Theta = \left(i\lambda\Omega - \Omega^2 + KS(|U|^2)\right)\mathrm{U} \tag{30}$$

By replacing expression of Θ from Equation 30 in equation 29, we obtain:

$$\frac{\partial N_u}{\partial\tau_1}(N_u) = -\frac{\Omega^2}{2Lg}\frac{A^2\lambda + \underline{c}_\theta\left[\lambda^2\Omega^2 + \left(KS(N_u^2) - \Omega^2\right)^2\right]}{\lambda^2\Omega^2 + 2KS'(N_u^2)\left(KS(N_u^2) - \Omega^2\right)N_u^2 + \left(KS(N_u^2) - \Omega^2\right)^2}N_u \tag{31}$$

From Equation 30, we write the expressions of $\dfrac{\partial N_\theta}{\partial N_u}$ and $\dfrac{\partial N_u}{\partial\tau_1}$ to calculate $\dfrac{\partial N_\theta}{\partial\tau_1}$:

$$\frac{\partial N_\theta}{\partial\tau_1}(\tau_1) = \frac{\partial N_\theta}{\partial N_u}\frac{\partial N_u}{\partial\tau_1}(\tau_1) \tag{32}$$

Figure 6a illustrates the variation of $\dfrac{\partial N_\theta}{\partial\tau_1}$ as a function of N_θ. It is seen that N_θ decreases abruptly to a considerable level and then it reduces its energy in an exponential manner. A numerical integration of the Equation 32 gives the theoretical evolution of N_θ as a function of time τ_1. One can see two distinct behaviours: the first one for $N_\theta > 0.2$ with an abrupt decrease in amplitude and the second one ($N_\theta < 0.2$), with an exponential manner.

This evolution is compared in Figure 6b with results obtained from the numerical integration of the system governing equations (see Equations 35, 36 and 37). The main difference

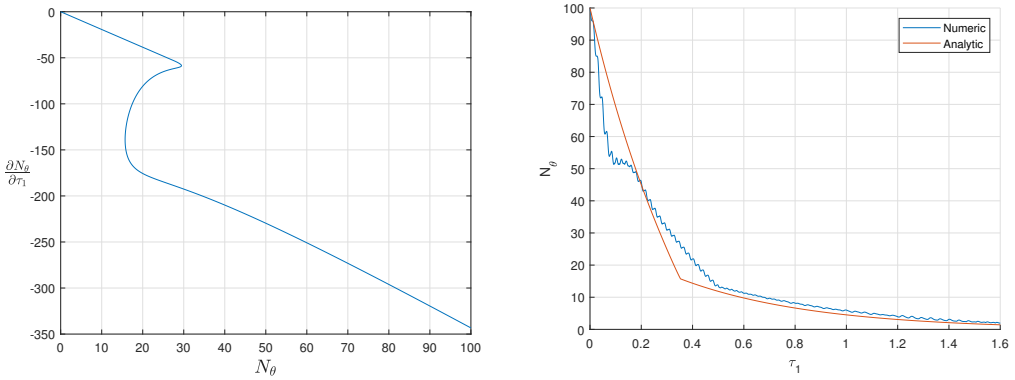

(a) Variation $\dfrac{\partial N_\theta}{\partial \tau_1}$ as a function of N_θ

(b) Comparison of analytic result to numerical integration.

Figure 6: Evolution of N_θ as a function of slow time τ_1.

is due to the approximation $\sigma = \sigma_\varphi + \varepsilon\sigma_{\sigma_\varphi} = \sigma_\psi + \varepsilon\sigma_{\sigma_\psi}$. In reality the frequencies ω_φ and ω_ψ are different and a phase angle δ increases over time. Since the SIM depends on δ, the behaviour of the NES and the variation of N_θ vary with δ.

2.7.3 Vertical excitation

In this case, there is only a vertical periodic motion of the base O. Here, a validation of the parameters of the NES is necessary to verify the possibility of existence of high amplitudes of the oscillations.

To understand the behaviour of the system, we consider $\Psi = 0$, $\underline{y}_1 = 0$, $\underline{x}_1 = 0$ and $\alpha = 0$, i.e. we consider a planar system. Here, the hypothesis of small Φ ($\Phi = \sqrt{\varepsilon}\underline{\Phi}$) would lead to irrelevant results. The Equation 25 leads to:

$$2iz_2L\Omega^3\Phi^* - \left(i\frac{2\sigma_\varphi Lg}{2} + \frac{\underline{c}_\varphi\Omega^2}{2}\right)\Phi - i\frac{A\Omega}{2}\left(a\Phi + \mathrm{U}\right) - i\frac{Lg}{16\Omega}\left|\Phi\right|^2\Phi = 0 \tag{33}$$

The equilibrium points of the system can be evaluated from Equations 23 and 33. They are shown in Figure 7. In previous study [16], we showed that the NES prevents the pendulum to reach high amplitude equilibrium point from a state with low amplitude.

It is worth to mention that in the design of the NES, the isolas should be treated and identified carefully as they could correspond to very high energy level of the main dofs and be counter-productive.

3 Tuning of parameters of the nonlinear absorber

To design the NES, we have to determine six parameters: the mass m, the position a, the angle α, the stiffness k, the clearance d and the damping coefficient c_u. These parameters have to be tuned to find good efficiency of the NES. These six parameters should be tuned all together. However, due to technical constraints, we suppose that the mass m and the position a of the NES are determined independently. The orientation angle α is also tuned independently because it depends on excitation and on the demand of the industry about the direction of the control.

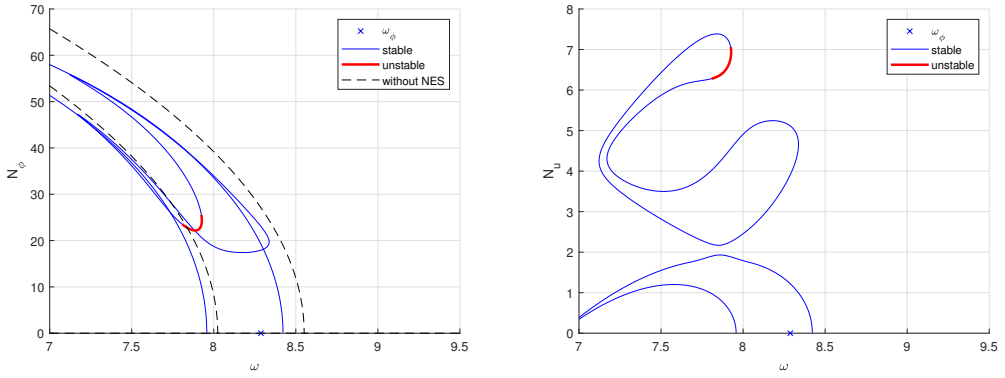

(a) N_φ (b) N_u

Figure 7: Equilibrium points of the system for a vertical excitation $z_2 = 0.05$.

3.1 The mass of the NES

The mass m does not appear directly in Equations 23, 25 and 26 but its effect is hidden behind the slow time scale $\tau_1 = \dfrac{m}{M}t$. Hence, the higher value of the mass m implies that the infinity of slow time scale τ_1 starts faster, i.e. the system can reach its equilibrium points faster [21]. However, due to the main assumptions in analytical developments ($\varepsilon \ll 1$) and due to technical constraints, m cannot be too high.

3.2 The position of the NES

The position of the NES is also determined by technical constraints, but several options can exist. In Equations 25 and 26, the decreasing of Φ and Ψ relative to slow time τ_1 due to the absorber is proportional to $A = a\Omega^2 - g$. In order to maximize A, the absorber has to be placed as far as possible from G, the equivalent mass center of the pendulum:

$$\vec{OG} = -\frac{g}{\Omega^2}\vec{k} \tag{34}$$

3.3 Orientation angle of the NES

In order to understand the effect of the orientation of the NES, we fix α the orientation angle of the NES and we study the response of the system for variable angles of horizontal base excitation, $\beta = \tan\left|\dfrac{y_1}{x_1}\right|$. Figure 8 shows the results for angle $\alpha \in [0, \dfrac{\pi}{2}]$. Here are some remarks:

1. It is confirmed that with $\alpha \neq 0 + j\dfrac{\pi}{2}$, $j \in \mathbb{Z}$, the NES can be efficient and can control both φ and ψ angles [14].
2. If $\alpha \to 0$, then the NES is not efficient in controlling φ. If $\alpha \to \dfrac{\pi}{2}$, then the NES is not efficient in controlling ψ.
3. If the direction of excitation β is known, then setting $\alpha = \beta$ provides a good control of the pendulum since both angles φ and ψ have relatively low amplitude.

3.4 Parameters maps

3.4.1 Horizontal excitation

Let us suppose that parameters m, a, α are already determined and we would like to find the good combination of parameters k, d and c. To do this, we build parameter maps in the plan (k, d) for several values of c with the amplitudes of angles φ and ψ.

This is performed by numerical integration of the equations of the system (Equations 35, 36 and 37). We simulate the system with horizontal base excitation $x_1 = 17\,\text{mm}$ from initial condition with no energy ($\varphi(0) = \psi(0) = u(0) = \dot{\varphi}(0) = \dot{\psi}(0) = \dot{u}(0) = 0$). The time of simulation is long enough to reach the asymptotic state of fast time: $\tau_0 = 100$.

Figure 9 shows the parameters maps for the amplitudes N_φ and N_ψ. The zone where the NES is more efficient is for low values of λ and d with the frequency $\sqrt{\frac{k}{m}}$ being close to the frequencies ω_φ and ω_ψ. This fact is similar to the design logic of a tuned mass damper. However, the zone of efficiency is very narrow and the absorber is not robust. In fact, as the main system is nonlinear, the frequencies of oscillations vary with the amplitude. Furthermore, it is technologically difficult to ensure a precise and low value of damping because of different phenomena such as friction, interactions, etc... So we prefer to take higher values of c_u and d to provide more robustness to the NES.

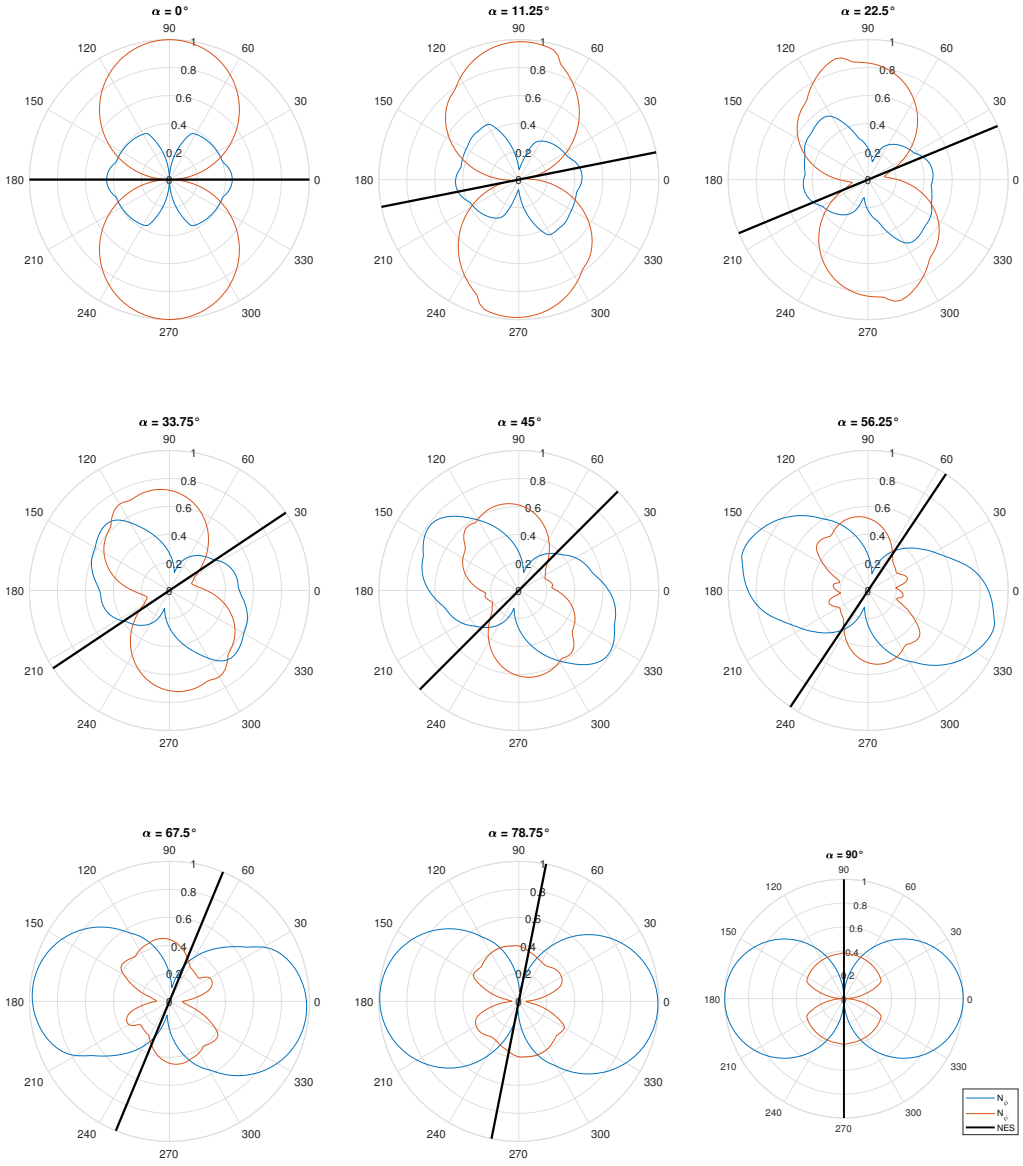

Figure 8: Amplitude of φ and ψ as a function of angle of applied horizontal base excitation (β) for several values of NES orientation (α).

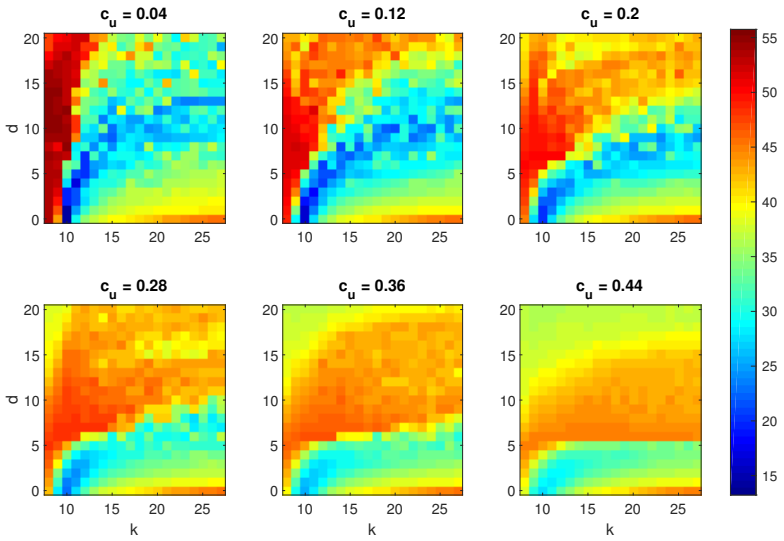

(a) Maximal value of N_φ

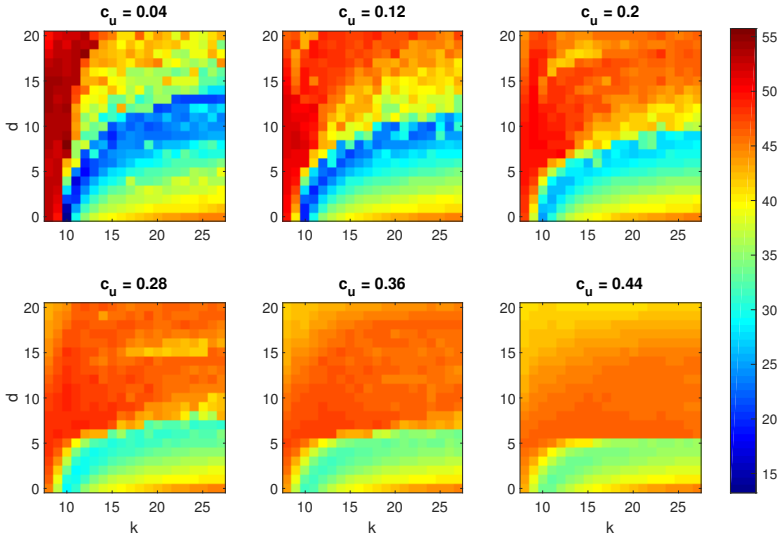

(b) Maximal value of N_ψ

Figure 9: Maximal value of N_φ and N_ψ for the system with parameters k, d and c_u and excited by horizontal base displacement ($x_1 = 17\,\mathrm{mm}$). Color scale corresponds to the maximal amplitude the system can reach for angles φ and ψ.

3.4.2 Initial energy

In this case, we would like to minimize the time t_c for which the system decreases its amplitude from an initial state to half of it. To evaluate this time, we consider Equation 29. For each combination of parameters (k, d, c_u), a numerical integration of the equation 32 is performed with an initial energy $N_\theta = 100$. Figure 10 shows the time t_c needed for the system to reach 50 % of its initial amplitude. We can observe following aspects:

- when the damping λ increases, the clearance d decreases;
- the NES is still efficient for high values of stiffness k.

To design a robust NES we choose a value of clearance d for which high values of stiffness k provide a good control.

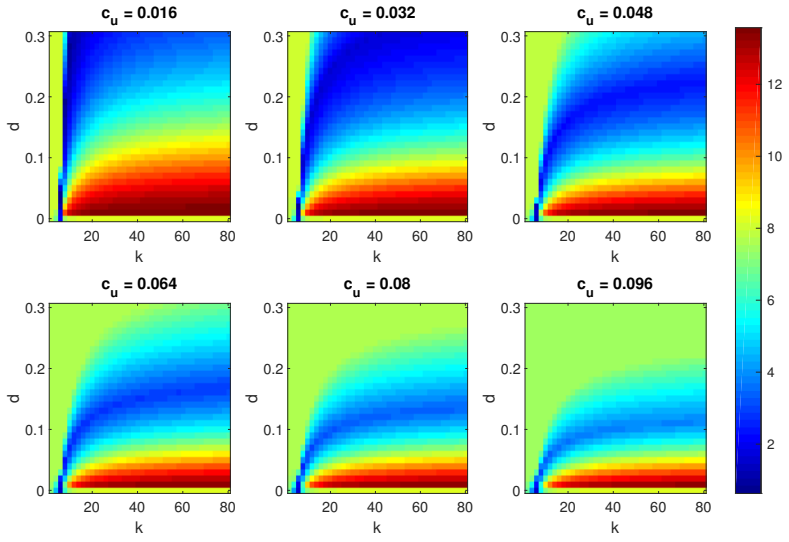

Figure 10: Time t_c (s) to reach 50 % of the initial amplitude as a function of parameters k, d and c_u.

4 Experimental validation

4.1 The prototype

A pendulum is made of a threaded rod. A parallelepiped of steel gives inertia in both directions. The hinge is made of two pivot linkages allowing the pendulum to rotate around $\vec{i}$ and $\vec{j}$ axes (see Figure 11b). The system is excited by the shake table. The values of x_1 and y_1 are set with the amplitude of acceleration of the shaker and the angle β between the table and the pendulum. It is possible to change the configuration of the shaker to excite the pendulum vertically and provide vertical displacement of the base $z_O(t)$ (see Figure 12).

The mass of the NES consists of a translating rod (via two linear ball bearings for minimizing friction), between two linear springs (see Figure 11a). For simulating the tests without NES, the mobile mass is blocked.

The parameters of the pendulum and the NES are those displayed on Table 1.

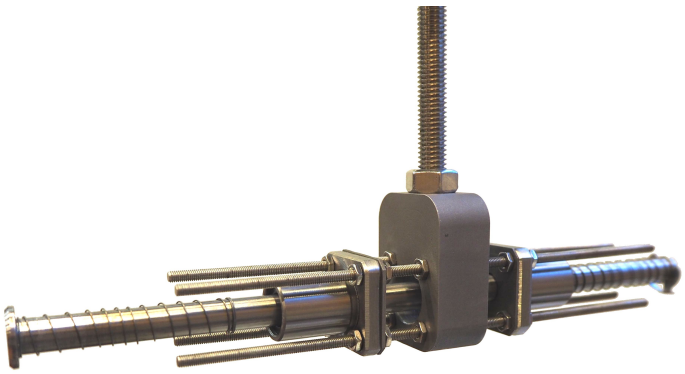

(a) Experimental piece-wise linear NES.

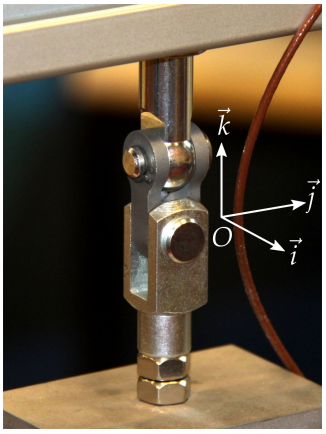

(b) Ball joint made of two pin joints.

Figure 11: Details of the experimental setup: (a) the NES is made by a rod moving between two springs; (b) the ball joint is made with two pin joints.

4.2 The test procedure

The tests consist of sinusoidal excitations with sweeping frequencies. The sweeping is carried out with increasing and decreasing frequencies. An uni-axial accelerometer measures the acceleration of the base O. The amplitude of excitation is ensured with a control loop. A triaxial accelerometer is glued on the pendulum which provides the values of angles φ and ψ. We excite the system with constant velocity amplitude of the base O for two reasons:

- compared to the test with constant acceleration, constant velocity reduces the displacement of the table at low frequencies ;
- the shake table provides the same power to the system independently of the frequency.

For these reasons, the amplitude of acceleration of the base is proportional to the frequencies.

4.3 Preliminary tests

Some preliminary tests are performed to characterize the system. As far as the system is nonlinear, several tests with different amplitudes of excitation are performed. The results are presented in Figure 13. It can be seen that:

- The frequency at the peak response decreases when the excitation increases. The main system presents a nonlinear softening behaviour.
- The shape of the curve with increasing and decreasing frequencies are very different. The system follows the stable branch of the response curve. When it meets an unstable state, it jumps on the other stable branch.

4.4 Horizontal base excitation

A test with and without the NES is performed with $\alpha = \beta = 0$. As shown in Figure 14, the NES reduces the amplitude of the pendulum with a factor of 2. To prove the efficiency of the NES on both angles φ and ψ, another test is performed with $\alpha = \frac{\pi}{4}$. The results shown in Figure 15 show the NES is still efficient.

(a) Horizontal excitation (b) Vertical excitation

Figure 12: Pictures of the experimental setup: a pendulum hung to a jib crane and excited by an electrodynamical shaker in horizontal (a) or vertical (b) directions.

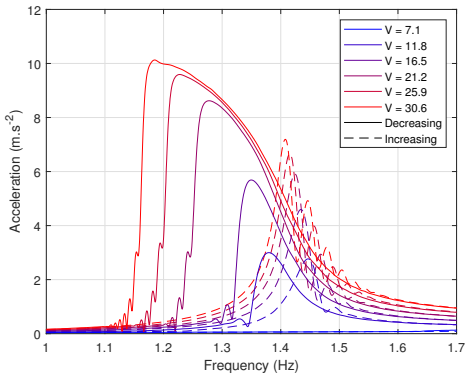

Figure 13: Response of the pendulum to several amplitudes of excitation with $\alpha = \beta = 0$. Velocity amplitude V are given in $\mathrm{mm\,s^{-1}}$.

4.5 Vertical base excitation

The shaker of the table is oriented vertically to give a vertical displacement at the base O. It is necessary to give an initial energy at the pendulum in order to create oscillations of the system. This is done by an initial angle θ. Figure 16 shows that without NES, the pendulum reaches a state with high amplitude of oscillations. With the NES, the system goes rapidly to the equilibrium point $N_\theta = 0$. This confirms that the NES is efficient for the vertical base excitation.

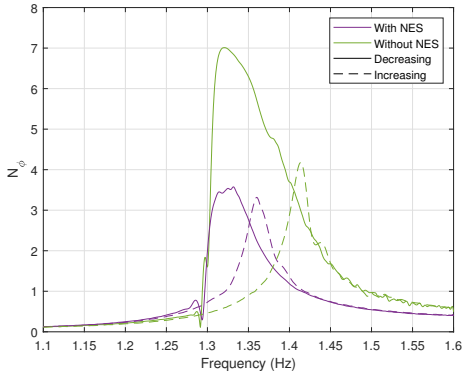

Figure 14: Test result with $\alpha = \beta = 0$ with and without NES.

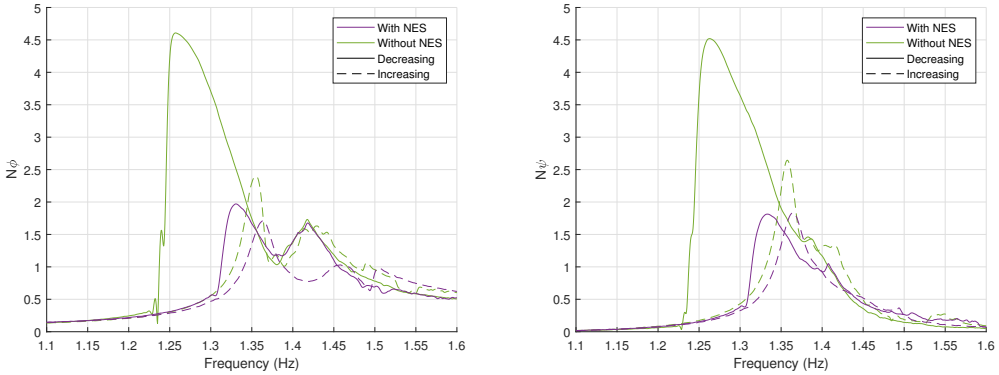

(a) N_φ (b) N_ψ

Figure 15: Test result with $\alpha = \pi/4$ and $\beta = 0$ with and without NES for amplitudes of angles φ and ψ.

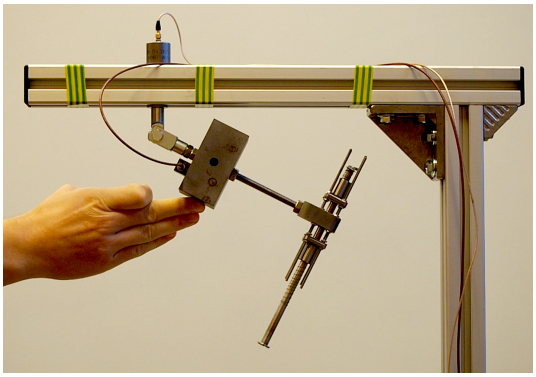

(a) Initial energy given to the pendulum.

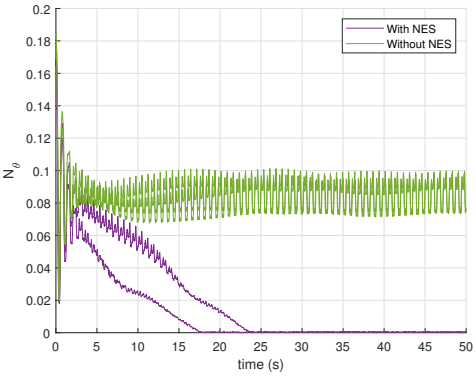

(b) Evolution of θ amplitude.

Figure 16: Comparison of the response of the pendulum with and without NES, with vertical excitation and initial energy.

5 Conclusion

We propose a method to design a nonsmooth nonlinear energy sink to control a two degrees-of-freedom pendulum for three types of excitations: horizontal base excitation, vertical base excitation and the initial energies. First we analysed the governing equations of a mathematical model of the system with a time multiple scale method. Thanks to this analysis, we can evaluate the efficiency of the control process by the NES under each of three types of excitations. The design process consists of tuning six parameters of the nonsmooth absorber. The mass, the position and the orientation angle are first fixed due to the technical constraints. Then, the good combinations of the stiffness, clearance and damping of the nonlinear energy sink are found with parameters maps taking account the robustness of the device.

Finally, the proposed design tools are tested on a prototype pendulum mounted on the shake table. The tests show that the nonlinear energy sink is efficient to control the oscillation of the pendulum. The explained procedure in this paper provides design tools for passive control of pendulum type systems, such as gondola lifts, by nonsmooth absorber. Obtained results in this paper (theoretical and experimental) will be used to design a nonlinear system for controlling pendulum movements of full-scale gondola lift.

Acknowledgement This research was funded by "La Région Auvergne Rhone Alpes" in the frame of the CALIPSO project.

Author contributions All authors of this paper have contributed equally in its different scientific aspects (analytical and numerical developments, discussion of results, etc.) and also in writing the article.

Data availability statement Research data are not shared.

A Equations of the system

$$
\begin{aligned}
&\varepsilon\cos(\alpha)^2\ddot{\varphi}u^2+\left[L^2+\varepsilon a^2+\frac{I_{xx}}{M}\right]\ddot{\varphi}+\varepsilon\cos(\alpha)\cos(\varphi)\sin(\alpha)\ddot{\psi}u^2+a\varepsilon\sin(\alpha)\sin(\varphi)\ddot{\psi}u\\
&\quad+a\varepsilon\cos(\alpha)\ddot{u}+2\varepsilon\cos(\alpha)^2\dot{\varphi}\dot{u}u+c\varphi\varepsilon\dot{\varphi}-\varepsilon\cos(\alpha)^2\cos(\varphi)\sin(\varphi)\dot{\psi}^2u^2\\
&\quad+\left[2a\varepsilon\cos(\alpha)\cos(\varphi)^2-a\varepsilon\cos(\alpha)\right]\dot{\psi}^2u+\left[\cos(\varphi)\sin(\varphi)L^2+\varepsilon\cos(\varphi)\sin(\varphi)a^2\right]\dot{\psi}^2\\
&\quad+2\varepsilon\cos(\alpha)\cos(\varphi)\sin(\alpha)\dot{\psi}\dot{u}u+2a\varepsilon\sin(\alpha)\sin(\varphi)\dot{\psi}\dot{u}+\left[\ddot{z}_O\varepsilon\cos(\alpha)\cos(\varphi)\cos(\psi)\right.\\
&\quad\left.-\ddot{x}_O\varepsilon\cos(\alpha)\sin(\varphi)+\varepsilon g\cos(\alpha)\cos(\varphi)\cos(\psi)-\ddot{y}_O\varepsilon\cos(\alpha)\cos(\varphi)\sin(\psi)\right]u\\
&\quad+\left[L\cos(\varphi)+a\varepsilon\cos(\varphi)\right]\ddot{x}_O-\left[a\varepsilon\sin(\varphi)\sin(\psi)+L\sin(\varphi)\sin(\psi)\right]\ddot{y}_O\\
&\quad+\left[L\cos(\psi)\sin(\varphi)+a\varepsilon\cos(\psi)\sin(\varphi)\right]\left[g+\ddot{z}_O\right]+Lg\cos(\psi)\sin(\varphi)=0
\end{aligned}
\tag{35}
$$

$$
\begin{aligned}
&\varepsilon\cos(\alpha)\cos(\varphi)\sin(\alpha)\ddot{\varphi}u^2+a\varepsilon\sin(\alpha)\sin(\varphi)\ddot{\varphi}u+\left[\varepsilon-\varepsilon\cos(\alpha)^2\cos(\varphi)^2\right]\ddot{\psi}u^2+c\psi\varepsilon\dot{\psi}\\
&\quad-2a\varepsilon\cos(\alpha)\cos(\varphi)\sin(\varphi)\ddot{\psi}u+\left[L^2\cos(\varphi)^2+\varepsilon a^2\cos(\varphi)^2+\frac{I_{yy}}{M}\right]\ddot{\psi}+a\varepsilon\cos(\varphi)\sin(\alpha)\ddot{u}\\
&\quad-\varepsilon\cos(\alpha)\sin(\alpha)\sin(\varphi)\dot{\varphi}^2u^2+a\varepsilon\cos(\varphi)\sin(\alpha)\dot{\varphi}^2u+2\varepsilon\cos(\alpha)^2\cos(\varphi)\sin(\varphi)\dot{\varphi}\dot{\psi}u^2\\
&\quad+\left[2a\varepsilon\cos(\alpha)-4a\varepsilon\cos(\alpha)\cos(\varphi)^2\right]\dot{\varphi}\dot{\psi}u+\left[-2\cos(\varphi)\sin(\varphi)L^2-2\varepsilon\cos(\varphi)\sin(\varphi)a^2\right]\dot{\varphi}\dot{\psi}\\
&\quad+2\varepsilon\cos(\alpha)\cos(\varphi)\sin(\alpha)\dot{\varphi}\dot{u}u+\left[2\varepsilon-2\varepsilon\cos(\alpha)^2\cos(\varphi)^2\right]\dot{\psi}\dot{u}u-2a\varepsilon\cos(\alpha)\cos(\varphi)\sin(\varphi)\dot{\psi}\dot{u}\\
&\quad+\left[-\varepsilon\sin(\alpha)\sin(\psi)-\varepsilon\cos(\alpha)\cos(\psi)\sin(\varphi)+L\cos(\varphi)\cos(\psi)+a\varepsilon\cos(\varphi)\cos(\psi)\right]\ddot{y}_O\\
&\quad+\left[\varepsilon\cos(\psi)\sin(\alpha)u-\varepsilon\cos(\alpha)\sin(\varphi)\sin(\psi)u+a\varepsilon\cos(\varphi)\sin(\psi)+L\cos(\varphi)\sin(\psi)\right]\left[g+\ddot{z}_O\right]=0
\end{aligned}
\tag{36}
$$

$$
\begin{aligned}
&a\varepsilon\cos(\alpha)\ddot{\varphi}+a\varepsilon\cos(\varphi)\sin(\alpha)\ddot{\psi}+\varepsilon\ddot{u}-\varepsilon\cos(\alpha)^2\dot{\varphi}^2u-2\varepsilon\cos(\alpha)\cos(\varphi)\sin(\alpha)\dot{\varphi}\dot{\psi}u\\
&\quad-2a\varepsilon\sin(\alpha)\sin(\varphi)\dot{\varphi}\dot{\psi}+\left[\varepsilon\cos(\alpha)^2\cos(\varphi)^2-\varepsilon\right]\dot{\psi}^2u+a\varepsilon\cos(\alpha)\cos(\varphi)\sin(\varphi)\dot{\psi}^2\\
&\quad+c\varepsilon\dot{u}+s(u)+\varepsilon\cos(\alpha)\cos(\varphi)\ddot{x}_O+\left[\varepsilon\cos(\psi)\sin(\alpha)-\varepsilon\cos(\alpha)\sin(\varphi)\sin(\psi)\right]\ddot{y}_O\\
&\quad+\left[\varepsilon\cos(\alpha)\cos(\psi)\sin(\varphi)+\varepsilon\sin(\alpha)\sin(\psi)\right]\left[g+\ddot{z}_O\right]=0
\end{aligned}
\tag{37}
$$

References

[1] George W Housner, Lawrence A Bergman, T Kf Caughey, Anastassios G Chassiakos, Richard O Claus, Sami F Masri, Robert E Skelton, TT Soong, BF Spencer, and James TP Yao. "Structural control: past, present, and future". *Journal of engineering mechanics* 123.9 (1997), pp. 897–971 (cit. on p. 1).

[2] Hermann Frahm. "Device for damping vibrations of bodies." Pat. US Patent 989,958. 1911 (cit. on p. 1).

[3] Robert E. Roberson. "Synthesis of a nonlinear dynamic vibration absorber". *Journal of the Franklin Institute* 254.3 (1952), pp. 205–220. DOI: 10.1016/0016-0032(52)90457-2 (cit. on p. 1).

[4] A. F. Vakakis and O. Gendelman. "Energy Pumping in Nonlinear Mechanical Oscillators: Part II. Resonance Capture". *Journal of Applied Mechanics* 68.1 (2001), p. 42. DOI: 10.1115/1.1345525 (cit. on p. 1).

[5] O. Gendelman, L. I. Manevitch, A. F. Vakakis, and R. M'Closkey. "Energy Pumping in Nonlinear Mechanical Oscillators: Part I-Dynamics of the Underlying Hamiltonian Systems". *Journal of Applied Mechanics* 68.1 (2001), p. 34. DOI: 10.1115/1.1345524 (cit. on p. 1).

[6] Young S. Lee, Alexander F. Vakakis, Lawrence A. Bergman, and D. Michael McFarland. "Suppression of limit cycle oscillations in the van der Pol oscillator by means of passive non-linear energy sinks". *Structural Control and Health Monitoring* 13.1 (2006), pp. 41–75. DOI: 10.1002/stc.143 (cit. on p. 1).

[7] Oleg V. Gendelman. "Targeted energy transfer in systems with non-polynomial nonlinearity". *Journal of Sound and Vibration* 315.3 (2008), pp. 732–745. DOI: 10.1016/j.jsv.2007.12.024 (cit. on pp. 1, 5).

[8] C.-H. Lamarque, O. V. Gendelman, A. Ture Savadkoohi, and E. Etcheverria. "Targeted energy transfer in mechanical systems by means of non-smooth nonlinear energy sink". *Acta Mechanica* 221.1-2 (2011), pp. 175–200. DOI: 10.1007/s00707-011-0492-0 (cit. on pp. 1 sq.).

[9] Mathieu Weiss, Mahmoud Chenia, Alireza Ture Savadkoohi, Claude-Henri Lamarque, Bastien Vaurigaud, and Abdelaziz Hammouda. "Multi-scale energy exchanges between an elasto-plastic oscillator and a light nonsmooth system with external pre-stress". *Nonlinear Dynamics* 83.1-2 (2016), pp. 109–135. DOI: 10.1007/s11071-015-2314-8 (cit. on p. 1).

[10] Xilin Lu, Zhongpo Liu, and Zheng Lu. "Optimization design and experimental verification of track nonlinear energy sink for vibration control under seismic excitation". *Structural Control and Health Monitoring* 24.12 (2017). DOI: 10.1002/stc.2033 (cit. on p. 1).

[11] Matteo Izzi, Luca Caracoglia, and Salvatore Noè. "Investigating the use of Targeted-Energy-Transfer devices for stay-cable vibration mitigation". *Structural Control and Health Monitoring* 23.2 (2016), pp. 315–332. DOI: 10.1002/stc.1772 (cit. on p. 1).

[12] Mathieu Weiss, Bastien Vaurigaud, Alireza Ture Savadkoohi, and Claude-Henri Lamarque. "Control of vertical oscillations of a cable by a piecewise linear absorber". *Journal of Sound and Vibration* 435 (2018), pp. 281–300. DOI: 10.1016/j.jsv.2018.07.033 (cit. on p. 1).

[13] Hiroshi Matsuhisa, Rongrong Gu, Yongjing Wang, Osamu Nishihara, and Susumu Sato. "Vibration Control of a Ropeway Carrier by Passive Dynamic Vibration Absorbers". *JSME international journal. Ser. C, Dynamics, control, robotics, design and manufacturing* 38.4 (1995), pp. 657–662. DOI: 10.1299/jsmec1993.38.657 (cit. on p. 1).

[14] Gabriel Hurel, Alireza Ture Savadkoohi, and Claude-Henri Lamarque. "Nonlinear vibratory energy exchanges between a two degrees-of-freedom pendulum and a nonlinear absorber." *Journal of Engineering Mechanics* 145.8 (2019), p. 04019058. DOI: 10.1061/(ASCE)EM.1943-7889.0001620 (cit. on pp. 1, 4, 7, 10).

[15] Gabriel Hurel, Alireza Ture Savadkoohi, and Claude-Henri Lamarque. "Passive control of a two degrees-of-freedom pendulum by a non-smooth absorber". *Nonlinear Dynamics* 98.4 (2019), pp. 3025–3036. DOI: 10.1007/s11071-019-04891-0 (cit. on pp. 1, 3 sq., 6).

[16] Gabriel Hurel, Alireza Ture Savadkoohi, and Claude-Henri Lamarque. "Nonlinear passive control of a pendulum submitted to base excitations". *Acta Mechanica* 232.4 (2021), pp. 1583–1604. DOI: 10.1007/s00707-020-02916-z (cit. on pp. 2, 4, 9).

[17] Alireza Ture Savadkoohi, Claude-Henri Lamarque, and Zoran Dimitrijevic. "Vibratory energy exchange between a linear and a nonsmooth system in the presence of the gravity". *Nonlinear Dynamics* 70.2 (2012), pp. 1473–1483. DOI: 10.1007/s11071-012-0548-2 (cit. on p. 2).

[18] L. I. Manevitch. "The Description of Localized Normal Modes in a Chain of Nonlinear Coupled Oscillators Using Complex Variables". *Nonlinear Dynamics* 25.1 (2001), pp. 95–109. DOI: 10.1023/A:1012994430793 (cit. on p. 4).

[19] Ali Hasan Nayfeh and Dean T. Mook. *Nonlinear oscillations*. Wiley classics library ed. Wiley classics library. New York, 1995 (cit. on p. 4).

[20] Y. Starosvetsky and O.V. Gendelman. "Strongly modulated response in forced 2DOF oscillatory system with essential mass and potential asymmetry". *Physica D: Nonlinear Phenomena* 237.13 (2008), pp. 1719–1733. DOI: 10.1016/j.physd.2008.01.019 (cit. on p. 7).

[21] C.-H. Lamarque, A. Ture Savadkoohi, E. Etcheverria, and Z. Dimitrijevic. "Multi-scale dynamics of two coupled nonsmooth systems". *International Journal of Bifurcation and Chaos* 22.12 (2012), p. 1250295. DOI: 10.1142/S0218127412502951 (cit. on p. 10).